Eigenvalues of the sample covariance matrix for a towed array

Peter Gerstoft,[a] Ravishankar Menon, and William S. Hodgkiss
Scripps Institution of Oceanography, University of California San Diego, La Jolla, California 92093-0238

Christoph F. Mecklenbräuker
Institute of Telecommunications, Vienna University of Technology, 1040 Vienna, Austria

(Received 30 March 2012; revised 17 July 2012; accepted 27 July 2012)

It is well known that observations of the spatial sample covariance matrix (SCM, also called the cross-spectral matrix) reveal that the ordered noise eigenvalues of the SCM decay steadily, but common models predict equal noise eigenvalues. Random matrix theory (RMT) is used to derive and discuss properties of the eigenvalue spectrum of the data SCM for linear arrays, with an application to ocean acoustic data. Noise on the array is considered either incoherent or propagating acoustic noise that is coherent across the array. Using conventional three-dimensional or two-dimensional isotropic noise models with full or snapshot-deficient observations, realizations of the SCM eigenvalues are explained using RMT. Deep-water towed-array data are analyzed and it is shown that the eigenvalues of the SCM compare well with theory. It is demonstrated how RMT can be applied to study eigenvalue spectrum estimation as dependent on array properties (element spacing to wavelength ratio) and data sampling (snapshots). Apart from explaining the observed noise eigenvalue spectrum, the improved model of the eigenvalue spectrum has important applications in array signal processing.
 [http://dx.doi.org/10.1121/1.4746024]

PACS number(s): 43.60.Fg, 43.60.Cg [ZHM] Pages: 2388–2396

I. INTRODUCTION

Often the ocean acoustic data sample covariance matrix (SCM, or cross-spectral matrix) is assumed to consist of a few large signal-plus-noise eigenvalues followed by a set of equal-value noise-only eigenvalues representing uncorrelated noise. However, it is well known that the SCM from real data observations is characterized by steadily decaying noise-only eigenvalues.

In array processing, a common rule of thumb is that the SCM is "well-estimated" when the number of snapshots is 2 to 3 times the array dimension.[1–3] This depends on the type of noise and application under consideration. Often, the number of snapshots available for forming the SCM is less than this, especially for large arrays.[4–10]

Using random matrix theory (RMT)[11,12] to model the statistical properties of the SCM,[13–19] the eigenvalue distributions are more informative than using the expectation alone. A random matrix is a matrix-valued random variable, i.e., the elements are stochastic variables. RMT can be used to study the distribution of eigenvalues under asymptotic assumptions. Using RMT, it can be shown that the eigenvalues have well-defined statistical properties. For acoustics, RMT has found applications in, e.g., elastodynamics[20] and wave propagation and scattering in random media.[21–24]

Using tools from RMT, we study the asymptotic behavior of the SCM eigenvalues under the assumption that both the sample size (snapshots) and number of sensors tends to infinity while their ratio is constant. This is in contrast to taking the mean of the SCM where sample size (snapshots) tends to infinity while the number of sensors is constant. Initially, RMT was developed assuming uncorrelated observations, with the distribution of the SCM eigenvalues given by the Marčenko–Pastur (MP) density.[25] More relevant for ocean acoustic applications, both the coherent and the incoherent noise components in the observations can be modeled in the SCM via a complex Wishart distribution.

This paper discusses the SCM eigenvalue decay structure focusing on the coherent noise component using simulations and real data and thus motivates further studies using RMT. Using RMT, it might be possible to model the convergence of the SCM and design improved eigenvalue based array-processing algorithms.

II. NOISE COVARIANCE MATRIX (CM)

The SCM is defined as

$$\hat{\Sigma} = \frac{1}{M}\sum_{m=1}^{M} \mathbf{x}_m \mathbf{x}_m^H, \tag{1}$$

where $\mathbf{x}_m, m = \{1, \ldots, M\}$ is the N-element complex-valued observation vector at a particular frequency f and M the number of snapshots. We are interested in the eigendecomposition of the SCM with ordered eigenvalues $\lambda_1 \geq \cdots \geq \lambda_N$, the eigenvalue spectrum.

Using a linear model

$$\mathbf{x} = \sum_{k=1}^{K} S_k \mathbf{s}_k + \mathbf{n}_c + \mathbf{n}_i, \tag{2}$$

where $\mathbf{n}_i \sim \mathcal{CN}(\mathbf{0}, \sigma_i^2 \mathbf{I})$ represents incoherent noise, i.e., sensor self-noise and $\mathbf{n}_c \sim \mathcal{CN}(\mathbf{0}, \sigma_c^2 \Sigma_c)$ represents coherent propagating noise between sensors with the diagonal elements of Σ_c normalized to 1. There are $K \ll N$ discrete sources from direction s_k with complex amplitude S_k.

[a]Author to whom correspondence should be addressed. Electronic mail: gerstoft@ucsd.edu

 0001-4966/2012/132(4)/2388/9/$30.00

Assuming $\mathbf{s}_k$, $\mathbf{n}_c$, and $\mathbf{n}_i$ are uncorrelated, the CM is

$$\Sigma = E(\mathbf{x}\mathbf{x}^H) = \sum_{k=1}^{K} |S_k|^2 \mathbf{s}_k \mathbf{s}_k^H + \sigma_c^2 \Sigma_c + \sigma_i^2 \mathbf{I}. \quad (3)$$

It is well known that the estimate Eq. (1) converges to Eq. (3) for $M \to \infty$ in a mean square sense. From this model it often is assumed that the first K eigenvalues contain signal-plus-noise and the remaining $N-K$ eigenvalues are just due to noise. In particular, for incoherent noise only, i.e., $\sigma_c^2 = 0$, all non-signal eigenvalues are equal-valued

$$\lambda_j = \sigma_i^2, \quad j = K+1, ..., N. \quad (4)$$

In the remainder it is assumed $K = 0$.

We have discussed Eq. (2) in terms of propagating coherent noise and non-propagating sensor noise. The incoherent noise is uncorrelated between the sensors but for certain array spacings the coherent noise also becomes uncorrelated.

The noise snapshot vector $\mathbf{n}_c + \mathbf{n}_i$ in Eq. (2) is modeled as a stationary, zero-mean, complex Gaussian stochastic process with covariance $\Sigma = \sigma_c^2 \Sigma_c + \sigma_i^2 \mathbf{I}$, i.e., $\mathbf{x}_m \sim \mathcal{CN}(\mathbf{0}, \Sigma)$. Based on this model, the SCM $\hat{\Sigma}$ in Eq. (1) is complex Wishart distributed with M degrees of freedom and covariance Σ, i.e., $M\hat{\Sigma} \sim \mathcal{W}_N(\sigma_c^2 \Sigma_c + \sigma_i^2 \mathbf{I}, M)$.

A. Statistical description of eigenvalues

The classical equal-valued eigenvalues for the incoherent noise Eq. (4) is derived based on the assumption that the system parameter (array size) N is constant and the number of snapshots $M \to \infty$. A full statistical description is obtained taking $\nu = N/M$ constant and then let $M \to \infty$ (i.e., N increases with M). This can be analyzed using RMT for incoherent or coherent[19] noise. For $\nu = 0$ the results correspond to the classical ensemble average.

The statistics of the SCM eigenvalues can be characterized by several distributions, such as:

(1) The joint distribution of the eigenvalues.[26]
(2) The distribution of the largest eigenvalue λ_1. For Wishart matrices, this is described by the Tracy–Widom density (when scaled and centered appropriately).[27]
(3) The distribution of the jth largest eigenvalue.[28]
(4) The empirical distribution of the eigenvalues, e.g., the MP distribution in Sec. II B 1.

For characterizing the noise, we are concerned with item (4).

The empirical cumulative distribution function (CDF) of the SCM eigenvalues is defined as

$$F(\lambda) = \frac{\#\{\lambda_j \le \lambda\}}{N}, \quad (5)$$

where # represents the cardinality of the set, i.e., the number of eigenvalues less than λ.

To give the empirical CDF a probabilistic interpretation, we define the random variable Λ which takes realizations from the finite set of eigenvalues $\{\lambda_1, \ldots, \lambda_N\}$ with uniform probability. Specifically, we define $\mathrm{P}\{\Lambda = \lambda_j\} = 1/N$ for all $j = 1, \ldots, N$ and

$$\mathrm{P}\{\Lambda \le \lambda\} = \sum_{j:\lambda_j \le \lambda} \mathrm{P}\{\Lambda = \lambda_j\} = F(\lambda). \quad (6)$$

Thus, the distribution of a uniformly selected eigenvalue is identical to the CDF.

The eigenvalue density of the SCM is defined as

$$p(\lambda) = \frac{1}{N} \sum_{j=1}^{N} \delta(\lambda - \lambda_j) = \frac{\mathrm{d}F(\lambda)}{\mathrm{d}\lambda}. \quad (7)$$

In the following, we examine $p(\lambda)$ for coherent and incoherent noise.

B. Incoherent noise

Array processing is typically performed under the assumption of uncorrelated noise between the sensors. Important early results in RMT are based on uncorrelated observations.

1. MP density

For noise that appears uncorrelated between the sensors, the snapshots are distributed as $\mathbf{n}_i \sim \mathcal{CN}(\mathbf{0}, \sigma_i^2 \mathbf{I})$. For $M \to \infty$ and $\nu = N/M$, $0 \le \nu \le 1$ constant (i.e., the number of elements N increases with M), the eigenvalues of the SCM $\hat{\Sigma}_i$ are distributed as given by the MP density[25]

$$\mathrm{p_{MP}}(\lambda) = \begin{cases} \dfrac{\sqrt{(l_+ - \lambda)(\lambda - l_-)}}{2\pi\nu\lambda\sigma_i^2} & l_- < \lambda < l_+ \\ 0 & \text{otherwise,} \end{cases} \quad (8)$$

where $l_- = \sigma_i^2(1 - \sqrt{\nu})^2$ and $l_+ = \sigma_i^2(1 + \sqrt{\nu})^2$ are the upper and lower limits of the "spreading" of the eigenvalues of the SCM around the true eigenvalue σ_i^2.

Figure 1(a) shows the MP density, Eq. (8), for $\sigma_i^2 = 1$ and $\nu = 1$, 1/4, and 1/25. The largest eigenvalue is about l_+ or 4, 9/4, and 36/25 times σ_i^2, illustrating how the density becomes narrower as ν decreases (M increases). For $\nu \to 0$ the MP density approaches a delta function at σ_i^2, in agreement with Eq. (4) for $K = 0$. The classical result for the expectation Eq. (3) corresponds to $\nu \to 0$.

2. Simulation of incoherent noise eigenvalues

The MP density Eq. (8) is only valid asymptotically, but this density works well for finite array size N and snapshots M as demonstrated in Figs. 1(b) and 1(c); see also Sec. II C 5 for the snapshot-deficient case. For finite N and M, realizations of the SCM can be generated from its distribution $M\hat{\Sigma} \sim \mathcal{W}_N(\sigma_i^2 \mathbf{I}, M)$. The simulations use a constant array size $N = 64$ and computes the SCM eigenvalues for $M = N$, $4N$, $25N$ (or $\nu = 1$, 1/4, 1/25). Figure 1(b) shows how the observed eigenvalues of the SCM are related to the MP density and Fig. 1(c) shows the conventional ordered display illustrating the decay of eigenvalues with eigenvalue index.

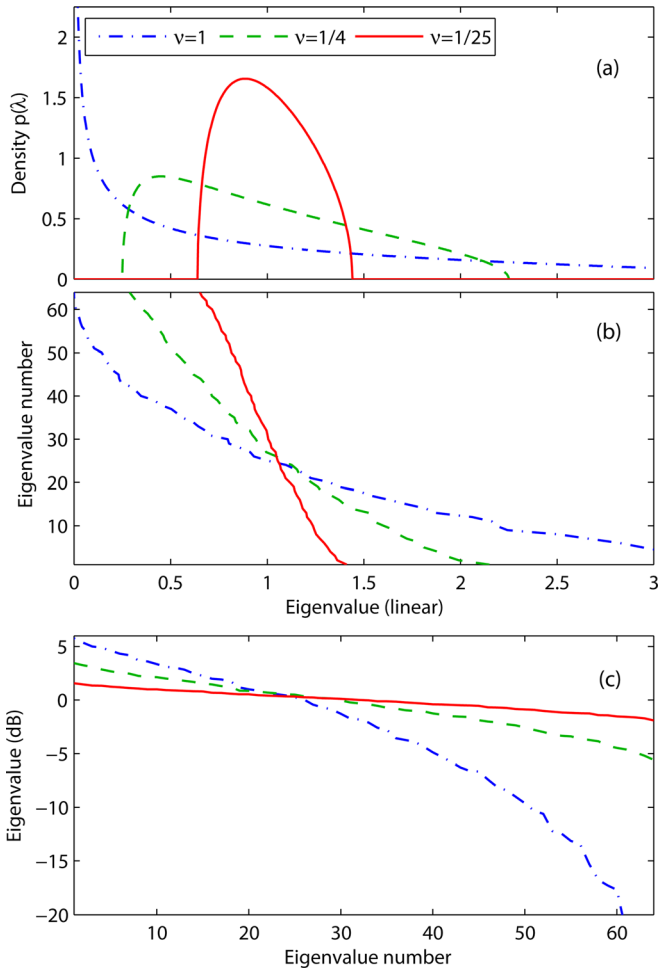

FIG. 1. (Color online) (a) Eigenvalue probability density of the incoherent noise SCM corresponding to a MP density Eq. (8) for $\sigma_i^2 = 1$ and $\nu = N/M = 1, 1/4, 1/25$. (b) and (c) Eigenvalues of the SCM for an array with $N = 64$ and number of snapshots M, $\nu = N/M = 1, 1/4, 1/25$. In (c) the axes are changed relative to (b) and the eigenvalue is in dB.

Clearly, as M increases, the eigenvalues approach the constant value given in Eq. (4). For real arrays the observation time is finite and often $M \approx N$ as the number of snapshots is limited by requiring a stationary environment.

C. Coherent noise

Environmental noise sources are coherent between pairs of sensors due to propagation effects in the ocean. This is in contrast to sensor noise which is incoherent and typically much lower in power than the environmental noise. Note that environmental noise may appear uncorrelated at specific element spacings (Sec. II B). For the three-dimensional (3D) isotropic noise model this occurs at half-wavelength spacing.

1. 3D isotropic noise eigenvalues

For a linear array of N equidistant sensors and assuming a 3D isotropic noise field, the elements of the coherent noise CM $\sigma_c^2 \Sigma_c^{3D}$ of the noise field are proportional to[19,29] (omitting σ_c^2)

$$[\Sigma_c^{3D}]_{ij} = \mathrm{sinc}(2\beta\,|\,i-j\,|), \tag{9}$$

where $\mathrm{sinc}(x) = \sin(\pi x)/(\pi x)$ and β is the ratio of the spacing between the sensors to the wavelength under consideration ($\beta = f\Delta x/c$, where f is the frequency, Δx is the spacing between the sensors, and c is the phase speed of wave propagation in the medium). Equation (9) is a symmetric Toeplitz matrix. Thus, the spatial correlations are only dependent on β and the separation $|i-j|$.

Asymptotically, the eigenvalues of a symmetric Toeplitz matrix are sampled from the Fourier transform of the sequence of elements that form the rows of the matrix.[30] Thus, asymptotically ($N \to \infty$), the eigenvalues of Σ_c^{3D} in Eq. (9) are proportional to the Fourier transform of the sinc function $\phi(\kappa)$, which is the rectangle function:

$$\phi(\kappa) = \frac{1}{2\beta}\,\mathrm{rect}\left(\frac{\kappa}{2\beta}\right), \tag{10}$$

where $\kappa \in [-1/2, 1/2)$ is the spatial frequency. Hence, the eigenvalues have at most two distinct values and for $\beta \leq 1/2$ just one non-zero value[19,31] with multiplicity ratio 2β (the multiplicity ratio is the identical number of eigenvalues relative to the array dimension).

For large but finite N, an approximate formula for the eigenvalues of Σ_c^{3D} can be obtained by sampling Eq. (10) at N points as in Eq. (11) and the 1/2 is introduced to obtain symmetry of the sampled eigenvalues.

$$\lambda_j^{3D} = \begin{cases} \dfrac{1}{2\beta} & \text{for} \quad \dfrac{j-1/2}{N} \leq 2\beta \\ 0 & \text{otherwise,} \end{cases} \tag{11}$$

where $j \in 1, \ldots, N$.

For $\beta < 1/2$, Σ_c^{3D} is rank deficient due to the zero eigenvalues of multiplicity ratio $(1-2\beta)$. For $\beta = 1/2$ (half-wavelength element spacing), $\Sigma_c^{3D} = I$ and thus $\lambda_j^{3D} = 1$, $j = 1, \ldots, N$ and Σ_c^{3D} is full rank.

Using the CM eigenvalues, the density for the eigenvalues of the SCM can be derived.[19] Since the CM has just one distinct non-zero eigenvalue, Eq. (11), the density is inferred from the MP density as follows. (1) The zero CM eigenvalues remain zero in the SCM. (2) As the multiplicity ratio of the non-zero eigenvalue is 2β as opposed to 1 for the MP density, the equivalent array element to snapshot ratio becomes $\tilde{\nu} = 2\beta\nu$. (3) Since the probability of obtaining a non-zero eigenvalue is 2β, the density of the non-zero eigenvalues is scaled by 2β. (4) Further, we need to scale the spread of the eigenvalues with $\sigma_c^2 1/2\beta$. This gives the coherent MP density

$$p_{c\mathrm{MP}}(\lambda) = \begin{cases} 2\beta\dfrac{\sqrt{(\lambda_+ - \lambda)(\lambda - \lambda_-)}}{2\pi\nu\lambda\sigma_c^2} & \lambda_- < \lambda < \lambda_+ \\ (1-2\beta)\delta(\lambda) & \text{otherwise,} \end{cases} \tag{12}$$

with

$$\lambda_\pm = \frac{\sigma_c^2}{2\beta}\,(1 \pm \sqrt{\tilde{\nu}})^2 = \sigma_c^2\left(\sqrt{\frac{1}{2\beta}} \pm \sqrt{\nu}\right)^2. \tag{13}$$

The first term in Eq. (12) accounts for the density due to the spreading of the non-zero eigenvalues and the second term in Eq. (12) is the density due to the zero eigenvalues.

2. 2D isotropic noise eigenvalues

For a two-dimensional (2D) isotropic noise field,[32] the coherent noise CM is proportional to

$$[\Sigma_c^{2D}]_{ij} = J_0\,(2\pi\beta\,|\,i-j\,|), \tag{14}$$

where J_0 is the zeroth order Bessel function. Since Σ_c^{2D} also is Toeplitz symmetric, its eigenvalues are samples from the Fourier transform of $J_0(2\pi\beta x)$:

$$\phi(\kappa) = \mathcal{F}[J_0(2\pi\beta x)] = \frac{\text{rect}\left(\frac{\kappa}{4\pi\beta}\right)}{\pi\beta\sqrt{1-(\kappa/2\pi\beta)^2}}, \tag{15}$$

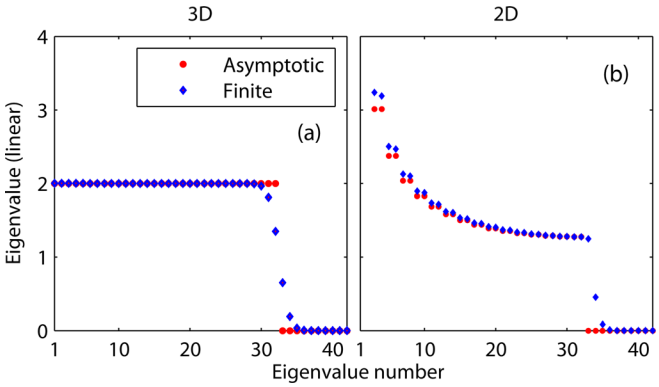

FIG. 2. (Color online) CM eigenvalues based on (a) 3D and (b) 2D isotropic noise for $\beta = 1/4$ and $N = 64$. The approximate eigenvalues [•, (a) Eq. (11) and (b) Eq. (16)] as well as the eigenvalues for a finite array (◆) are shown.

where $\kappa \in [-\pi, \pi)$ is the spatial frequency. Thus, similar to the 3D case, for finite N an approximate formula for the eigenvalues is obtained by sampling Eq. (15) and for $\beta \le 1/2$, the (unsorted) eigenvalues are given by

$$\lambda_j^{2D} = \begin{cases} \dfrac{1}{\pi\beta\sqrt{1-\left|\dfrac{j-(N+1)/2}{N\beta}\right|^2}} & \text{for } \left|\dfrac{j-(N+1)/2}{N}\right| \le \beta \\ 0 & \text{otherwise,} \end{cases} \tag{16}$$

where $j \in 1,\ldots,N$. These eigenvalues come in pairs due to the symmetry around $N/2$.

Similar to the 3D case for $\beta < 1/2$, Σ_c^{2D} is rank deficient due to the zero eigenvalues of multiplicity ratio $(1-2\beta)$ (asymptotically, $N \to \infty$) as shown in Eq. (16). The first zero of the Bessel function, $J_0(2\pi\beta x)$, for $x = 1$ occurs at $\beta = 0.38$, but successive zeros do not occur at multiples of 0.38 and hence their spacing is not periodic [although the asymptotic expansion $J_0(2\pi\beta x) \approx \sqrt{1/\pi^2\beta x}\ \cos(2\pi\beta x - \pi/4)$ suggests that the zeros occur periodically for large arguments]. Hence for a 2-sensor array,[32] the noise on the array is uncorrelated at $\beta = 0.38$, but for larger uniformly spaced arrays, the 2D isotropic noise SCM will never be uncorrelated, even at $\beta = 0.5$.

The CM eigenvalue spectrum for 3D and 2D isotropic noise is shown in Fig. 2 for $N = 64$ and $\beta = 1/4$. The CM eigenvalues are computed using eigenvalue decompostions on Σ_c [◆, Eqs. (9) and (14)] and the asymptotic formulas [•, Eqs. (11) and (16)], see Fig. 2. For the 2D case [Fig. 2(b)], the large eigenvalues come in pairs and eigenvalues 1 to 2 are beyond the limits of the plot. For finite N, there are a number of eigenvalues near the normalized eigenvalue index 2β (these are not in pairs), defining the edge of the visible region. The visible region of the array is where the eigenvectors correspond to element-to-element phase shifts of physically propagating waves in the medium.

The SCM eigenvalue density for 2D isotropic noise is not available analytically and is obtained from simulation as demonstrated in Sec. II C 3.

3. Simulation of coherent noise eigenvalues

The SCM eigenvalue densities are estimated numerically using Monte Carlo simulation and shown here for 3D and 2D isotropic noise for $N = 64$ and $\beta = 1/4$.

The SCMs are generated as $M\hat{\Sigma}_c \sim \mathcal{W}_N(\Sigma_c, M)$ and their ordered eigenvalues are shown in Figs. 3(a) and 3(c) for a single realization. The difference in structure between the SCM eigenvalues for 3D [Fig. 3(a)] and 2D [Fig. 3(c)] isotropic noise is pronounced for $\nu = 1/25$, mirroring the shapes of their respective asymptotic formulas for the CM eigenvalues [Eqs. (11) and (16)] as shown in Fig. 2. However, for $\nu = 1$ (dotted-dashed line) the spreading of the eigenvalues looks similar and it is difficult to distinguish between the two noise fields.

The empirical eigenvalue densities are obtained from 1000 Monte Carlo samples [Figs. 3(b) and 3(d)]. The 3D asymptotic distributions [Eq. (12)] for both $\nu = 1$ and $\nu = 1/25$ match well the finite dimension simulated distributions [Fig. 3(b)].

For $\nu = 1/25$, the main density is quite sharply centered around $1/2\beta = 2$ for the 3D case as the underlying

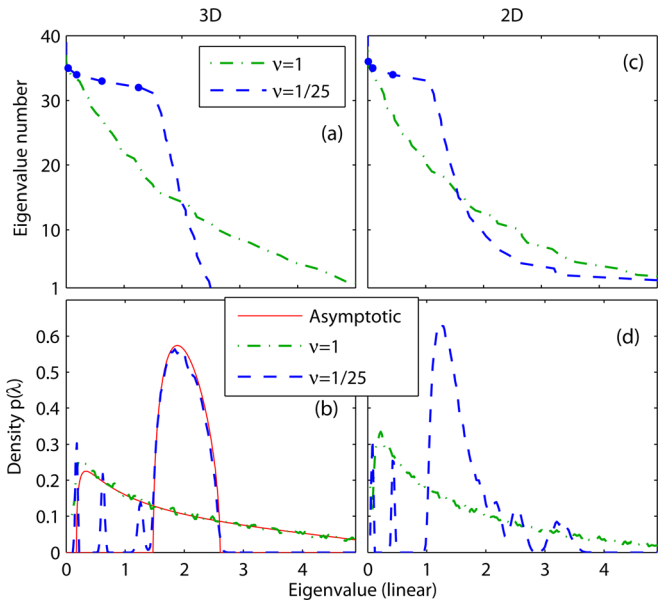

FIG. 3. (Color online) (a) and (c) SCM eigenvalues, and (b) and (d) SCM eigenvalue densities based on (a) and (b) 3D and (c) and (d) 2D isotropic noise for $\nu = N/M = 1$, 1/25. The simulation is performed with $N = 64$, $\beta = 1/4$, the SCM eigenvalues are based on one realization and the densities are obtained from 1000 Monte Carlo samples. In (b) the asymptotic densities [solid, Eq. (12)] are shown. In (b) and (d) the probability mass of $1 - 2\beta = 0.5$ at $\lambda = 0$ is not shown.

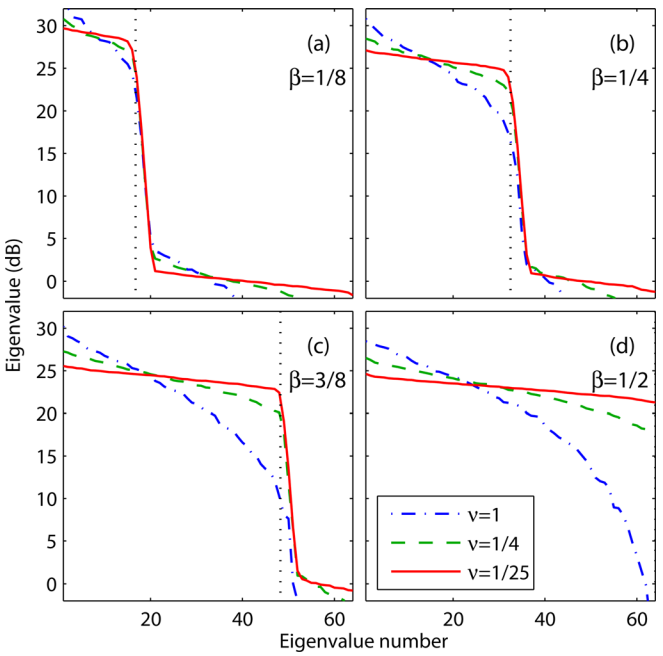

FIG. 4. (Color online) Eigenvalues of the SCM for the $N = 64$ element array with $\sigma_c^2/\sigma_i^2 = 200$ for: (a) $\beta = 1/8$, (b) $\beta = 1/4$, (c) $\beta = 3/8$, and (d) $\beta = 1/2$. The eigenvalues are shown for an increasing number of snapshots M, where $\nu = N/M = 1$ (dashed-dotted), $\nu = 1/4$ (dashed), and $\nu = 1/16$ (solid). The eigenvalues are normalized with σ_i^2 and the vertical dotted line indicates the edge of the visible region.

CM only has equal-valued eigenvalues of value $1/2\beta$ for $\beta \leq 1/2$, whereas the 2D density is more distributed. The localized peaks in the densities for both 3D (3 peaks) and 2D (2 peaks) observed for $\lambda < 1.5$ correspond to the "transition eigenvalues" which occur due to the finite dimension of Σ_c, the density for $\lambda < 0.05$ is suppressed. The transition eigenvalues of a single realization $\hat{\Sigma}_c$ (•) in Figs. 3(a) and 3(c) agree well with the peaks in the densities in Figs. 3(b) and 3(d).

For 2D isotropic noise and $\nu = 1/25$, there are several localized modes at larger eigenvalues ($\lambda > 2$). These corresponds to the eigenvalue pairs 3 to 4 ($\lambda \approx 3.3$), 5-6 ($\lambda \approx 2.5$), and 7 to 8 ($\lambda \approx 2.2$) of Σ_c^{3D} in Fig. 2(c) (eigenvalues 1 to 2 have $\lambda > 5$).

4. Simulation of coherent plus incoherent noise eigenvalues

To demonstrate the decay of the eigenvalues, we are interested in realizations of the noise SCM and their eigenvalues. Since the noise SCM is complex Wishart distributed $M\hat{\Sigma} \sim \mathcal{W}_N(\sigma_c^2\Sigma_c + \sigma_i^2\mathbf{I}, M)$ we can generate realizations of the SCM from which the eigenvalues are determined.

This is illustrated with simulations for an array with 64 elements with noise-only data. The coherent noise is chosen by a factor 200 larger than the incoherent noise, $\sigma_c^2/\sigma_i^2 = 200$. The simulations in Fig. 4 show the decay of the eigenvalues for all SCMs. As the number of snapshots is increased (with array size fixed, ν decreasing), the smaller eigenvalues become larger and eventually for an infinite number of snapshots the eigenvalues will approach a step function. The larger eigenvalues are dominated by the coherent noise and the smaller eigenvalues by the incoherent noise.

The location of the jump depends on β, the ratio of array spacing to wavelength. For $\beta < 1/2$ there is a sharp drop in the vicinity of the eigenvalues corresponding to the edge of the visible region. For fewer snapshots this jump is smeared out. A smaller ratio σ_c^2/σ_i^2 reduces the jump. At $\beta = 1/2$ the coherent noise CM also is diagonal and thus identical to the classical case of only incoherent noise discussed in Sec. II B.

It is interesting to compare the largest eigenvalues of the SCM for 2D and 3D isotropic noise, see Fig. 5. For the same number of snapshots ($\nu = 1/4$), the largest eigenvalues for the 2D case are 4 dB larger than for the 3D case. At $\beta = 1/2$, the 2D noise CM is not diagonal (the Bessel

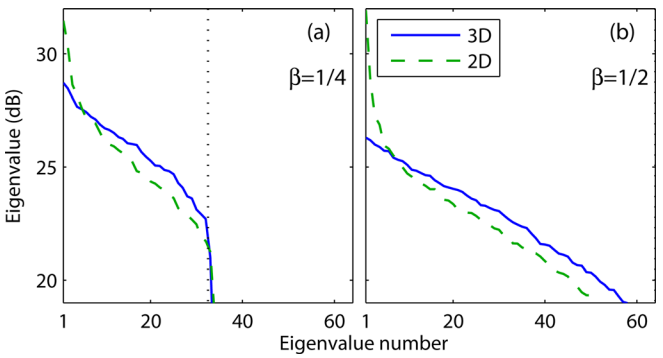

FIG. 5. (Color online) Eigenvalues of the 3D (solid) and 2D (dashed) noise SCM for an $N = 64$ element array with $\sigma_c^2/\sigma_i^2 = 200$, $\nu = 1/4$ for: (a) $\beta = 1/4$ and (b) $\beta = 1/2$. The eigenvalues are normalized with σ_i^2 and the vertical dotted line indicates the edge of the visible region.

function is not zero at $\beta = 1/2$) and eigenvalues are not similar to the incoherent case, see Fig. 1.

5. Snapshot-deficient case

If there are fewer snapshot samples than sensors ($M < N$, i.e., $\nu = N/M > 1$) the SCM has at most M eigenvalues and is said to be snapshot-deficient. This often is the case for large towed arrays or arrays in dynamic environments where the number of snapshots is limited.

For the snapshot-deficient incoherent-noise SCM, i.e., $M < N$, we can apply the MP density Eq. (8) with $\nu = N/M$ and adding a point mass of $1–1/\nu$ at $\lambda = 0$ corresponding to the $N–M$ zero eigenvalues. This can be derived as follows. All snapshots are collected into an $N \times M$ observation matrix $\mathbf{X} = [\mathbf{x}_1 \cdots \mathbf{x}_M]$. This gives the sample covariance matrices

$$\hat{\Sigma} = \frac{1}{M}\mathbf{X}\mathbf{X}^H \quad \text{and} \quad \hat{\Sigma}' = \frac{1}{N}\mathbf{X}^H\mathbf{X}, \tag{17}$$

where $M \times M$ matrix $\hat{\Sigma}'$ is only used in the derivation of the density, it is not a physical quantity. Since $\mathbf{X}$ is complex Gaussian $\mathcal{CN}_M(\mathbf{0}, \sigma_i^2\mathbf{I}_N)$ then $\mathbf{X}^H$ also is complex Gaussian $\mathcal{CN}_N(\mathbf{0}, \sigma_i^2\mathbf{I}_M)$. Both $\hat{\Sigma}$ and $\hat{\Sigma}'$ will be complex Wishart distributed, as $M\hat{\Sigma} \sim \mathcal{W}_N(\sigma_i^2\mathbf{I}_N, M)$ and $N\hat{\Sigma}' \sim \mathcal{W}_M(\sigma_i^2\mathbf{I}_M, N)$, respectively. Thus, the snapshot-deficient incoherent-noise SCM is given by the MP density $\hat{\Sigma}'$ matrix as if there were N "snapshots" and M "elements," provided a mass point of $1–1/\nu$ at $\lambda = 0$ is included to account for the zero eigenvalues.

For the snapshot-deficient 3D coherent-noise SCM, a simulation is used to obtain the eigenvalues. The snapshot-deficient SCM is simulated as in Sec. II C 4, but with just $M = 32$ snapshots, i.e., 32 non-zero eigenvalues, see Fig. 6. The eigenvalues decay faster for the snapshot-deficient SCM than when using more snapshots (solid versus dashed in Fig. 6). The snapshot-deficient case is further discussed in Sec. III.

III. EXPERIMENT

The data is from a towed horizontal array during the long range acoustic communications experiment[33] from 10:00 to 11:00 UTC on 16 September 2010 in the NE Pacific in 5-km water depth. Other data periods yield similar results to those shown here. The array was towed at 3.5 knots at a depth of 200 m. The data were sampled at 2000 Hz using a nested array with each configuration having 64 channels.[34] The high frequency (HF) array had hydrophone spacing 0.375 m (design frequency $f_d = 2000$ Hz), the medium frequency (MF) array had channel spacing 0.75 m ($f_d = 1000$ Hz), the low frequency (LF) array 1.5 m ($f_d = 500$ Hz), and the ultralow frequency (ULF) array 3 m ($f_d = 250$ Hz).

The SCMs were constructed using 4 s, 2^{13} long Fourier transforms without overlap and $M = 64$ ($\nu = 1$) or 864 ($\nu = 1/13$) snapshots, with 864 snapshots corresponding to the whole hour. The beamformed time series, Fig. 7, is based on single snapshots and performed at one quarter wavelength element spacing. The broad arrival at 60° to 75° is from the towship (R/V Melville). Apparently, the two arrivals at −45° and −30° come from distant transiting ships, although a log of ships in the area was not kept. Overall, the beam time series shows little change with time.

Figure 8 shows the eigenvalues of the SCM at selected values of β for the four arrays. Due to the low sampling frequency (2000 Hz), the HF array only can be used up to $\beta = 1/4$ (1000 Hz). All eigenvalues are based on 1 h observations, meaning that for $M = 64$ the eigenvalues are averaged over 13 SCM eigenvalues. The first few eigenvalues for each SCM are likely due to the distant transiting ships and noise from the towship, as seen in the beam time series (Fig. 7). The eigenvalues drop sharply above $2\beta(N-1)+1$ (vertical dotted line) as predicted by theory, and indicates that the coherent noise is stronger than the incoherent noise. The eigenvalues of the SCM of the LF and ULF arrays show a similar behavior as the MF and HF arrays though with less strong transition between the two eigenvalue regimes.

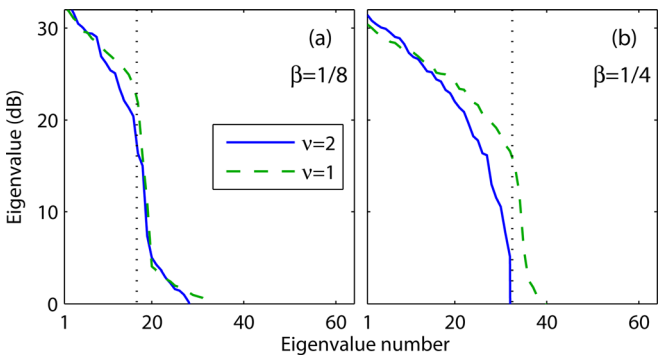

FIG. 6. (Color online) Eigenvalues of the snapshot-deficient SCM for a 64-element array for $M = 32$ (solid), i.e., $\nu = 2$ and $\sigma_c^2/\sigma_i^2 = 200$ for (a) $\beta = 1/8$ and (b) $\beta = 1/4$. For comparison, $M = 64$ (dashed, $\nu = 1$) also is shown. The eigenvalues are normalized with σ_i^2 and the vertical dotted line indicates the edge of the visible region.

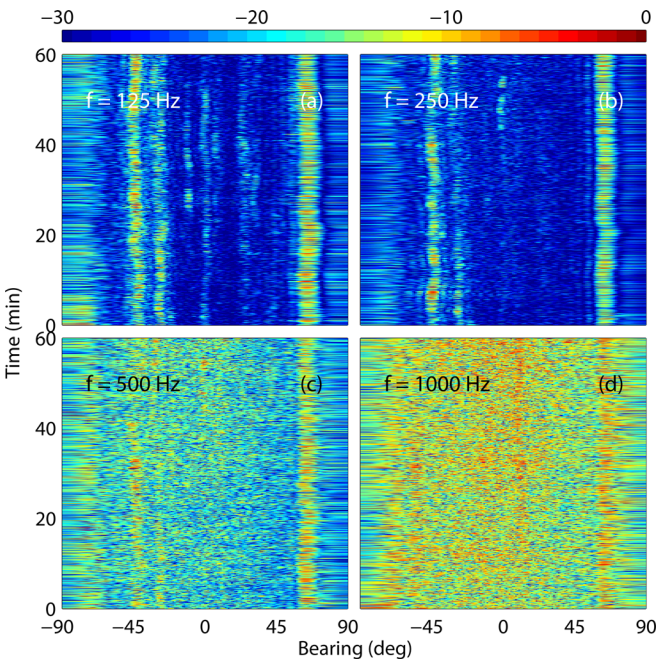

FIG. 7. (Color online) Towed array beam time series (dB) at one quarter wavelength element spacing: (a) ULF at 125 Hz, (b) LF at 250 Hz, (c) MF at 500 Hz, and (d) HF at 1000 Hz.

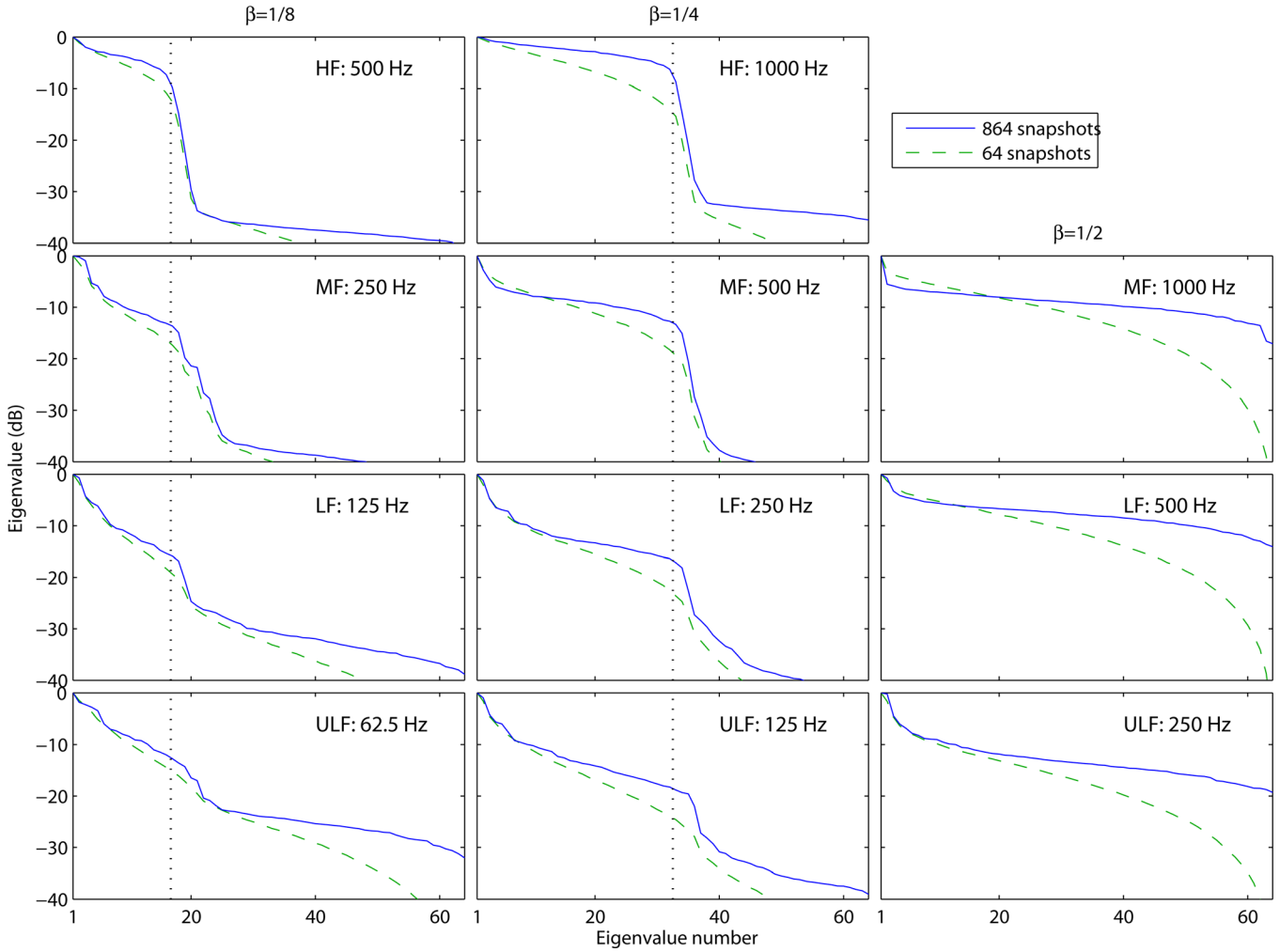

FIG. 8. (Color online) Eigenvalues of the towed array SCM for HF array (1st row, $\beta = 1/8, 1/4$), MF array (2nd row, $\beta = 1/8, 1/4, 1/2$), LF array (3rd row, $\beta = 1/8, 1/4, 1/2$), and ULF array (4th row, $\beta = 1/8, 1/4, 1/2$). The eigenvalues are based on 64 ($\nu = 1$, dashed) and 864 ($\nu = 13$, solid) snapshots. The eigenvalues are normalized with the largest eigenvalue and the vertical dotted line indicates the edge of the visible region, β is the element spacing to wavelength ratio.

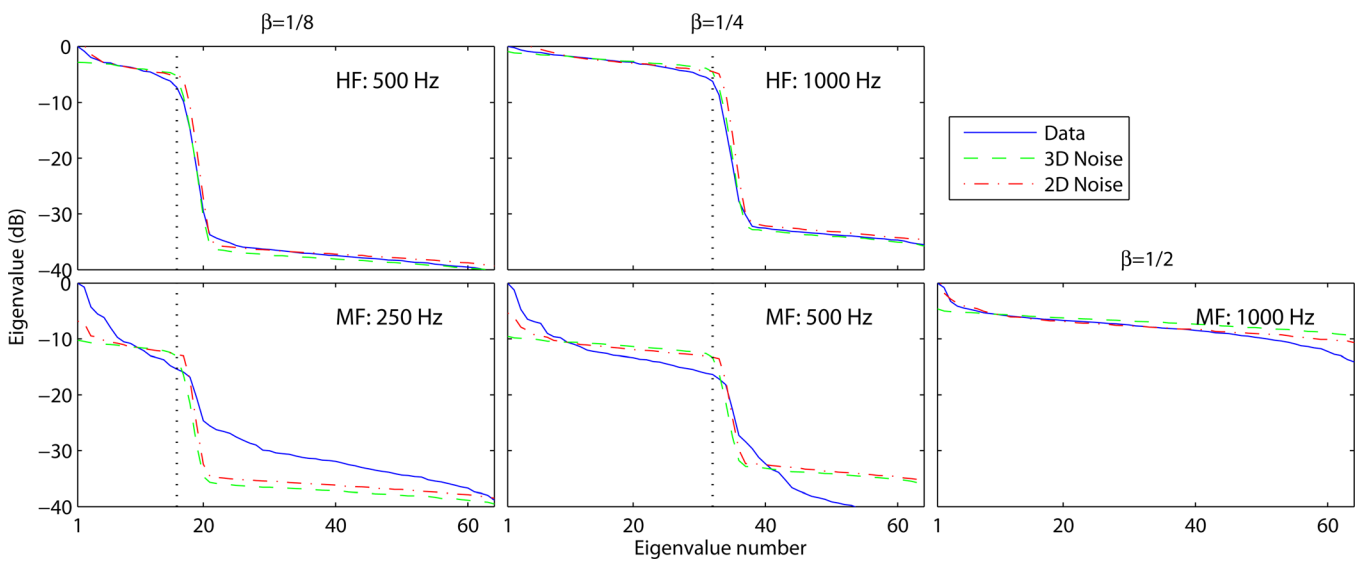

FIG. 9. (Color online) Comparison of observed and modeled eigenvalues. Eigenvalues of the towed array SCM (solid) and modeled eigenvalues 3D (dashed) and 2D (dashed-dotted) for HF array (1st row, $\beta = 1/8, 1/4$) and LF array (2nd row, $\beta = 1/8, 1/4, 1/2$). The observed eigenvalues are based on 864 ($\nu = 13$, solid) snapshots, the modeled eigenvalues use a ratio $\sigma_c^2/\sigma_i^2 = 700$ for the HF array and $\sigma_c^2/\sigma_i^2 = 100$ for the LF array. The eigenvalues are normalized with the largest eigenvalue and the vertical dotted line indicates the edge of the visible region, β is element spacing to wavelength ratio.

Figure 8 shows that the eigenvalues depend on β. As β increases, all the eigenvalue spectra become more extended and at $\beta = 0.5$ (half-wavelength spacing) the SCM ideally should become diagonal with eigenvalues that approximately are all equal.

Comparing the four arrays at $\beta = 1/8$, the first column in Fig. 8 shows that the higher eigenvalue numbers (containing mostly incoherent noise) are relatively larger at low frequencies. At half-wavelength spacing ($\beta = 1/2$, last column in Fig. 8), all eigenvalues remain large for the three arrays, except when using a relatively small number of snapshots ($M = N$).

The observed and modeled noise eigenvalues are compared in Fig. 9. It is important to realize that there is towship radiated noise as well as broadband signatures from several distant ships arriving at the array, especially at low frequencies, see Fig. 7. These "signals" are among the largest eigenvalues extracted from the data, see Eq. (2). Therefore, we arbitrarily select to only match the noise from eigenvalue 10 and vary the ratio of coherent to incoherent noise σ_c^2/σ_i^2, see Fig. 9. For the HF array, the match is quite good and the transition region is also well-determined. For the LF array, the match is less good, likely because not all dominant noise sources are modeled. Before these noise sources are understood, whether the noise field is 2D or 3D cannot be determined.

For large arrays, the SCM often is snapshot-deficient. The snapshot-deficient eigenvalues for the towed array data (Fig. 10) compare well with the simulations in Fig. 6. How well the coherent noise eigenvalues are estimated depends on β relative to the number of snapshots M. For small values of β, there might be sufficient snapshots so the coherent noise eigenvalues are relatively well estimated. An important question is how eigenvalue based beamforming performs for this case, but this is beyond the scope of this paper.

From all of the SCM eigenvalue spectra [Figs. 11(a) and 11(c)] we obtain histograms of the eigenvalues [Figs. 11(b) and 11(d)] corresponding to the empirical eigenvalue density, Eq. (7). Each SCM is normalized by the largest eigenvalue so that in the histograms the largest eigenvalues correspond to "signal" eigenvalues. The histograms are multi-modal corresponding to coherent and incoherent noise, as can also be seen from the second row in Fig. 8.

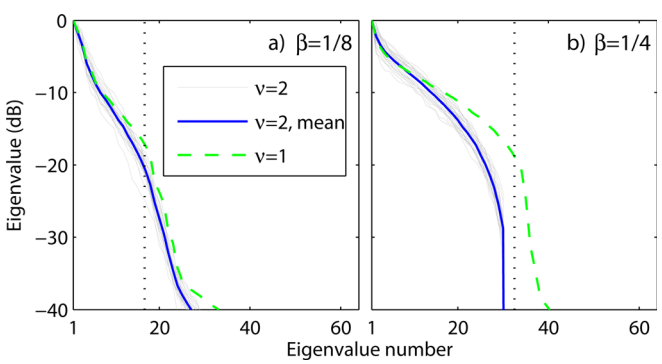

FIG. 10. (Color online) Eigenvalues of the MF towed array snapshot-deficient SCM with $M = 32$ $(\nu = 2)$ for several realizations (thin lines) for (a) $\beta = 1/8$ and (b) $\beta = 1/4$ (i.e., frequencies 500 and 1000 Hz). Average of these eigenvalues (solid) and eigenvalues of the SCM (dashed) with $M = N = 64$ $(\nu = 1)$ also are shown. The eigenvalues are normalized with the largest eigenvalue and the vertical dotted line indicates the edge of the visible region.

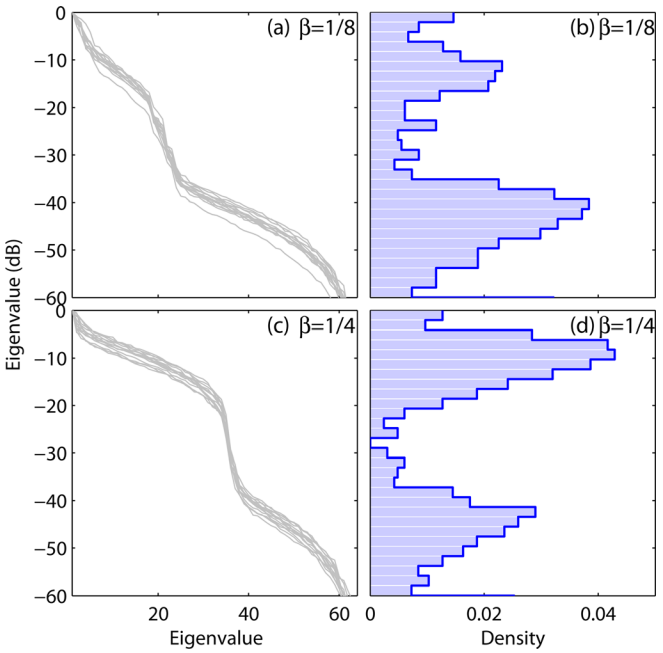

FIG. 11. (Color online) (a) and (c): Eigenvalues of the MF towed array SCM with $M = 64$ $(\nu = 1)$ for 13 realizations for (a) and (b) $\beta = 1/8$ (250 Hz) and (c) and (d) $\beta = 1/4$ (500 Hz). (b) and (d): The normalized histograms of all of the eigenvalues.

IV. CONCLUSION

Eigenvalue spectra of the SCM) have been examined for both synthetic and real data. The ordered eigenvalues decay steadily as predicted using RMT. Using tools from RMT, we study the asymptotic behavior of the SCM eigenvalues under the assumption that both the sample size and number of sensors tend to infinity while their ratio is constant. This is in contrast to taking the mean of the SCM where the sample size tends to infinity while the number of sensors is constant.

The noise observed by an equally-spaced line array has been modeled as the sum of an incoherent component and a stronger coherent component corresponding to propagating noise. The coherent component is modeled as 3D or 2D isotropic noise corresponding to a sinc or a zeroth-order Bessel CM. Eigenvalues of these were examined and both matrices were singular for element spacing to wavelength ratios less than 1/2, causing a sharp drop in the eigenvalues which is related to the edge of the visible region. Realizations of synthetic SCMs were drawn from the complex Wishart distribution in numerical simulations from which both eigenvalue spectra and densities were estimated.

Simulated and deep-water towed-array noise data SCMs clearly show the strong jump in power level at the edge of the visible region. Apart from this jump, the SCM eigenvalues decay steadily as predicted by theory. Snapshot deficient and well-estimated SCMs were considered.

ACKNOWLEDGMENT

The Office of Naval Research, Grant Nos. N00014-11-1-0321 and N00014-11-1-0320, supported this work.

[1]B. D. Carlson, "Covariance matrix estimation errors and diagonal loading in adaptive arrays," IEEE Trans. Aerosp. Electron. Syst. **24**, 397–401 (1988).
[2]I. S. Reed, J. D. Mallett, and L. E. Brennan, "Rapid convergence rate in adaptive arrays," IEEE Trans. Aerosp. Electron. Syst. **AES-10**, 853–863 (1974).
[3]D. E. Grant, J. H. Gross, and M. Z. Lawrence, "Cross-spectral matrix estimation effects on adaptive beamforming," J. Acoust. Soc. Am. **98**, 517–524 (1995).
[4]A. B. Baggeroer and H. Cox, "Passive sonar limits upon nulling multiple moving ships with large aperture arrays," in *Conference Record of the 33rd Asilomar Conference on Signals, Systems, and Computers*, Pacific Grove, CA (1999), Vol. 1, pp. 103–108.
[5]H. Song, W. A. Kuperman, W. S. Hodgkiss, P. Gerstoft, and J. Kim, "Null broadening with snapshot-deficient covariance matrices in passive sonar," IEEE J. Ocean. Eng. **28**, 250–261 (2003).
[6]T. C. Yang, "Motion compensation for adaptive horizontal line array processing," J. Acoust. Soc. Am. **113**, 245–260 (2003).
[7]P. Gerstoft, W. S. Hodgkiss, W. A. Kuperman, H. C. Song, M. Siderius, and P. L. Nielsen, "Adaptive beamforming of a towed array during a turn," IEEE J. Ocean. Eng. **28**, 44–54 (2003).
[8]D. Tollefsen, S. E. Dosso, and M. J. Wilmut, "Matched-field geoacoustic inversion with a horizontal array and low-level source," J. Acoust. Soc. Am. **120**, 221–230 (2006).
[9]J. S. Rogers and J. L. Krolik, "Time-varying spatial spectrum estimation with a maneuverable towed array," J. Acoust. Soc. Am. **128**, 3543–3553 (2010).
[10]S. D. Somasundaram and N. H. Parsons, "Evaluation of robust Capon beamforming for passive sonar," IEEE J. Ocean. Eng. **36**, 686–695 (2011).
[11]M. L. Mehta, *Random Matrices*, 3rd ed. (Academic Press, New York, 2004), Chap. 1.
[12]A. Edelman and N. R. Rao, "Random matrix theory," Acta Numerica **14**, 233–297 (2005).
[13]X. Mestre, "On the asymptotic behavior of the sample estimates of eigenvalues and eigenvectors of covariance matrices," IEEE Trans. Signal Process. **56**, 5353–5368 (2008).
[14]X. Mestre and M. A. Lagunas, "Modified subspace algorithms for DoA estimation with large arrays," IEEE Trans. Signal Process. **56**, 598–614 (2008).
[15]B. A. Johnson, Y. I. Abramovich, and X. Mestre, "MUSIC, G-MUSIC, and maximum-likelihood performance breakdown," IEEE Trans. Signal Process. **56**, 3944–3958 (2008).
[16]R. R. Nadakuditi and A. Edelman, "Sample eigenvalue based detection of high-dimensional signals in white noise using relatively few samples," IEEE Trans. Signal Process. **56**, 2625–2638 (2008).
[17]R. R. Nadakuditi and J. W. Silverstein, "Fundamental limit of sample generalized eigenvalue based detection of signals in noise using relatively few signal-bearing and noise-only samples," IEEE J. Sel. Top. Signal Process. **4**, 468–480 (2010).
[18]M. Pajovic, J. Preisig, and A. Baggeroer, "Analytical characterization of the MPDR-based power estimators in snapshot scarce regime," in *IEEE Stat. Signal Proc. Workshop* (Ann Arbor, MI, 2012), pp. 812–815; K. Wage, J. Buck, M. Dzieciuch, and P. Worcester, "Experimental validation of a random matrix theory model for dominant mode rejection beamformer notch depth," in *IEEE Stat. Signal Proc. Workshop* (Ann Arbor, MI, 2012), pp. 820–823; J. Buck and K. Wage, "A random matrix theory model for the dominant mode rejection beamformer notch depth," in *IEEE Stat. Signal Proc. Workshop* (Ann Arbor, MI, 2012), pp. 824–827; S. Tuladhar, J. Buck, and K. Wage, "Approximate eigenvalue distribution of a cylindrically isotropic noise sample covariance matrix," in *IEEE Stat. Signal Proc. Workshop* (Ann Arbor, MI, 2012), pp. 828–831.
[19]R. Menon, P. Gerstoft, and W. S. Hodgkiss, "Asymptotic eigenvalue density of noise covariance matrices," IEEE Trans. Signal Process. **60**, 3415–3424 (2012).
[20]R. L. Weaver, "Spectral statistics in elastodynamics," J. Acoust. Soc. Am. **85**, 1005–1013 (1989).
[21]R. R. Müller, "A random matrix model of communication via antenna arrays," IEEE Trans. Inf. Theory **48**, 2495–2506 (2002).
[22]A. Aubry and A. Derode, "Multiple scattering of ultrasound in weakly inhomogeneous media: Application to human soft tissues," J. Acoust. Soc. Am. **129**, 225–233 (2011).
[23]S. E. Skipetrov and A. Goetschy, "Eigenvalue distributions of large euclidean random matrices for waves in random media," J. Phys. A: Math. Theor. **44**, 065102 (2011).
[24]R. Menon, P. Gerstoft, and W. S. Hodgkiss, "Cross-correlations of diffuse noise in an ocean environment using eigenvalue based statistical inference," J. Acoust. Soc. Am. (in press), doi: 10.1121/1.4754558.
[25]V. A. Marčenko and L. A. Pastur, "Distributions of eigenvalues of some sets of random matrices," Math. USSR. Sb. **72**, 507–536 (1967).
[26]T. W. Anderson, *An Introduction to Multivariate Statistical Analysis*, 3rd ed. (Wiley-Interscience, Hoboken, NJ, 2003), Chap. 13.
[27]C. A. Tracy and H. Widom, "Level-spacing distributions and the Airy kernel," Commun. Math. Phys. **159**, 151–174 (1994).
[28]A. Zanella, M. Chiani, and M. Z. Win, "On the marginal distribution of the eigenvalues of Wishart matrices," IEEE Trans. Commun. **57**, 1050–1060 (2009).
[29]H. Cox, "Spatial correlation in arbitrary noise fields with application to ambient sea noise," J. Acoust. Soc. Am. **54**, 1289–1301 (1973).
[30]R. M. Gray, "Toeplitz and circulant matrices: A review," Found. Trends. Comm. Inf. Theory **2**, 155–239 (2006).
[31]D. Slepian, "Prolate spheroidal wave functions, Fourier analysis, and uncertainty—v: The discrete case," Bell Syst. Tech. J. **57**, 1271–1430 (1978).
[32]B. F. Cron and C. H. Sherman, "Spatial-correlation functions for various noise models," J. Acoust. Soc. Am. **34**, 1732–1736 (1962).
[33]H. C. Song, S. Cho, T. Kang, W. S. Hodgkiss, and J. R. Preston, "Long-range acoustic communication in deep water using a towed array," J. Acoust. Soc. Am. **129**, EL71–EL75 (2011).
[34]K. M. Becker and J. R. Preston, "The ONR five octave research array (FORA) at Penn State," in *Proceedings of the Oceans 2003 Marine Technology and Science Conference*, San Diego, CA (2003), Vol. 5, pp. 2607–2610.